WIRELINE FORMATION TESTING & WELL DELIVERABILITY

Contents

Chapter 2. Skin Factor in Perforated and Fractured Wells

Chapter 3. Well Inflow Performance Relations

Chapter 4. Gas Reservoir Material Balance

Chapter 5. General Mechanistic Reservoir Material Balance

Chapter 6. Coning and Displacement Models in the Material Balance Context

Chapter 7. Decline Curve Analysis

Chapter 8. Distributed Pressure Measurement

Chapter 9. Exploration Applications of Distributed Pressure Measurement

Chapter 10. Field Development Applications of Distributed Pressure Measurement

Chapter 11. Production Logging and Layered Systems

Chapter 12. Wireline Formation Testing (WFT) Permeability Interpretation

The following chapters are on the accompanying CD-ROM.

Chapter 13. Reservoir Engineering Aspects of Production

Chapter 14. Compartmentalized Material Balance

Chapter 15. Reservoir Characterization from Underbalanced Drilling Data

Chapter 16. Effect of Mud Filtrate Invasion on WFT Measured Pressure

Chapter 17. Tight Gas and Coal Bed Methane (CBM)

1

Radial Flow in Porous Media

Introduction

The basis of modern reservoir engineering lies in the quantitative description of unsteady-state, multiphase fluid flow in heterogeneous porous media under the influence of pressure as well as gravitational and capillary forces. In the general case, the flow pattern is spatially three dimensional and three separate phases—oil, water and gas—may be flowing simultaneously in the reservoir. Indeed, the complexity of the situation may be succinctly described by the statement:

- three dimensions
- three phases
- three forces

The solution of such formidable flow problems can be obtained only numerically using sophisticated simulation techniques. The only redeeming feature of reservoir flow is that it is essentially laminar in nature resulting in a linear relation between local superficial fluid velocity and potential gradient.

However, in certain circumstances the reservoir flow is much simpler in character and can be modeled on a reduced basis involving only one space dimension, one mobile phase, and one prevailing force. The best example of this approach is the radial flow which takes place in the vicinity of an individual well open to flow in the oil zone. Prior to any water breakthrough and provided the pressure is everywhere above the bubble point, the only flowing phase is oil. The connate water initially present is rendered immobile by capillary forces and the oil flow is determined solely by pressure gradient. The flow is essentially horizontal and, where water or gas coning is not appreciable, the one-dimensional assumption is a good approximation.

Radial flow in the vicinity of the well bore has a great influence on the productivity of a particular well. The well inflow model, which is the relation between the three key variables of flowing bottom-hole pressure, oil production rate, and average reservoir pressure, is the quantitative expression of productivity and it is the purpose of this treatment to develop such

This system, known as *darcy units*, and the SI system are consistent and no dimensional factors arise. Since most reservoir rocks have a permeability less than 1 darcy, the millidarcy (md) is often employed as a practical unit. However, another set of units called *reservoir* or *field units* is also widely used in which the quantities are expressed as follows:

q_s	: bbl/day (stock tank)	p	: psi
A	: ft^2	x	: ft
k	: md	μ	: cp

This system is not consistent, and Darcy's law takes the form

$$\frac{q_s B}{A} = -\frac{1.127\times10^{-3}k}{\mu}\cdot\frac{dp}{dx} \tag{1–8}$$

for horizontal flow; here B is the oil formation volume factor and the quantity q_sB is simply the in situ volumetric flow rate q. The unit conversion constant of 1.127×10^{-3} or its reciprocal 887.2 frequently occurs in equations involving Society of Petroleum Engineers (SPE) field units. The ratio k/μ entering Eq. (1–8), which is a combination of a rock property and a fluid property, is known as the *mobility*.

Darcy's law, i.e., Eq. (1–7), is the low-Reynolds-number limit of the more general flow in porous media equation due to Forcheimer:

$$\frac{dp}{dx} = -\frac{\mu}{k}u_r - \beta\rho u_r^2 \tag{1–9}$$

where β is a second rock property termed the *inertial resistance coefficient*, which has dimensions of L^{-1}, e.g., ft^{-1} in field units. The first term on the right-hand side of Eq. (1–9) is the viscous component, while the second term is the non-Darcy component. The non-Darcy term is important only if $\beta\rho u_r$ is comparable to μ/k, i.e., if

$$Re'' = \frac{k\beta\rho u_r}{\mu} > 0.1 \tag{1–10}$$

Here, Re'' is a modified Reynolds number for porous media. This condition is only ever satisfied for fluids of low viscosity near the wellbore where the velocity is high. The physical interpretation of non-Darcy flow has been elucidated by Sketne,[2] who has shown that the inertial (acceleration) terms in the Navier–Stokes equation for laminar flow in a porous medium become important at Reynolds numbers, based on the pore throat dimension, greater than unity. The nature of the motion in a porous medium is illustrated in figure 1–5, where the proper fluid dynamic definition of darcy flow is seen to be creeping laminar flow; there is no question of turbulence being involved in porous medium situations. Non-darcy flow near the sandface in gas wells is the origin of the rate-dependent skin factor treated later in this chapter.

In some circumstances, it is useful to know the volume-averaged pressure within the system, defined by

$$\bar{p} = \frac{\int pdV}{V} = \frac{\int_{r_w}^{r_e} p2\pi\, rhdr}{\pi r_e^2 h} \tag{1–36}$$

Substituting Eq. (1–35) into Eq. (1–36) and carrying out the necessary integration gives the following result:

$$\bar{p} = p_w + \frac{q\mu}{2\pi kh}\left(ln\frac{r_e}{r_w} - \frac{1}{2}\right) \tag{1–37}$$

Thus in steady-state radial flow, the difference between the mean pressure $\bar{p}$ and the external pressure p_e is small and is given by

$$p_e - \bar{p} = \frac{1}{2} \cdot \frac{q\mu}{2\pi kh} \tag{1–38}$$

i.e., a dimensionless pressure difference of one half. The concept of average pressure in steady-state radial flow is illustrated in figure 1–18.

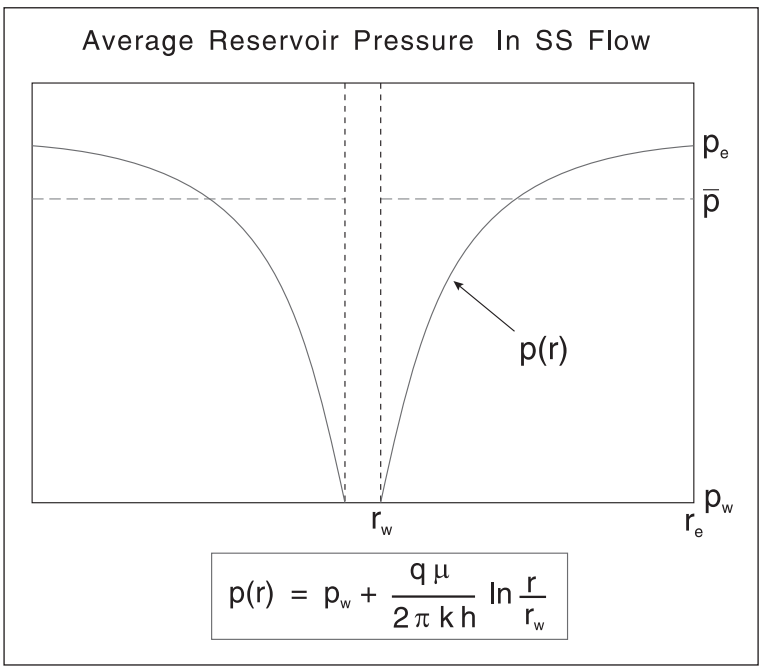

Fig. 1–18. Average pressure in steady-state flow

and the pressure at radius r is given by the equivalent formula

$$q = \frac{2\pi kh\,(p - p_w)}{\mu\left(ln\frac{r}{r_w} - \frac{r^2}{2r_e^2} + \frac{r_w^2}{2r_e^2}\right)} \qquad \textbf{(1–62)}$$

For $r_e >> r_w$, which is the usual case, then (1–61) may be written as

$$q = \frac{2\pi kh\,(p_e - p_w)}{\mu\left(ln\frac{r_e}{r_w} - \frac{1}{2}\right)} \qquad \textbf{(1–63)}$$

This is the well inflow equation under SSS conditions. The pressure profile and flow distribution for SSS flow are shown in figure 1–30. In terms of dimensionless overall drawdown, Eq. (1–63) may be written as

$$\frac{p_e - p_w}{\frac{q\mu}{2\pi kh}} = p_{De} = ln\, r_{De} - \frac{1}{2} \qquad \textbf{(1–64)}$$

Surprisingly, the difference between the pressure profile in SS and SSS flow is not great. Considering Eq. (1–62), it is obvious that for r close to r_w the term $r^2 / 2r_e^2 - r_w^2 / 2r_e^2$ is very small indeed and the two profiles are indistinguishable. The overall drawdown is greater for SS flow because the well production q passes unchanged through the whole radial zone; quantitatively, Eq. (1–64) shows that the dimensionless overall drawdown in SS flow exceeds that in SSS flow by one half, which is not much when $ln r_{De}$ is of the order of 8, say.

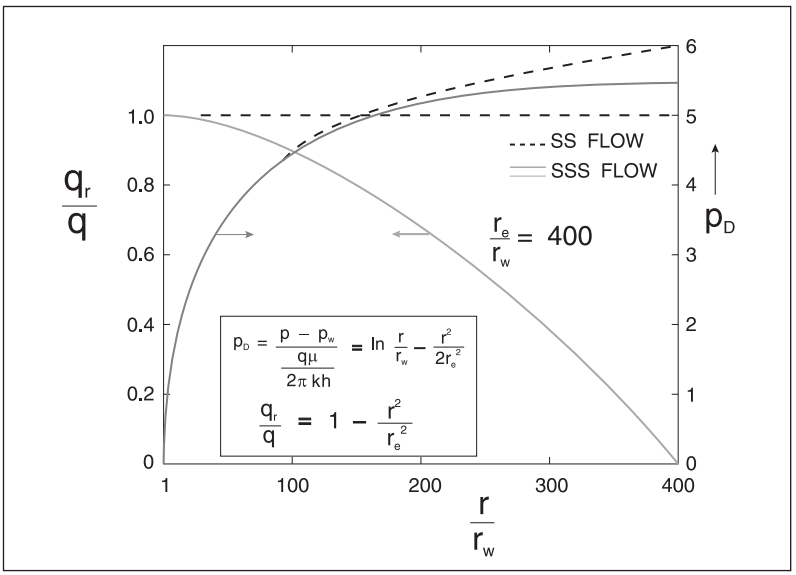

Fig. 1–30. Dimensionless pressure profile and flow distribution in SSS radial flow

and the expressions for productivity index become

$$J_{SS} = \frac{2\pi kh}{B\mu\left(ln\frac{r_e}{r_w} + S_{pr}\right)} \quad \text{or} \quad J_{SSS} = \frac{2\pi kh}{B\mu\left(ln\frac{r_e}{r_w} - \frac{3}{4} + S_{pr}\right)} \qquad \textbf{(1–130)}$$

This illustrates how the skin factor concept can be extended to allow for the deviation from pure radial flow which occurs in the vicinity of a fractured well and how the well PI is improved by stimulation. These formulae can be modified to include the Dietz shape factor for noncircular drainage areas and asymmetric well locations provided the fracture dimension x_f is small compared to the dimensions of the drainage area.

Horizontal Wells

Horizontal well spanning a rectangular drainage area

It is possible to define a PI for a horizontal well in a closed reservoir compartment or drainage area in SSS depletion. Since the dominant flow regime in the case of a horizontal well is linear flow, it is convenient to focus attention on the closed rectangle as a useful geometry for elucidation of well productivity index; the geometry is illustrated in figure 1–67. It should be emphasized that it may take a long time for an SSS distribution to develop, particularly in low-permeability reservoirs. The PI discussed here is a late-time descriptor. In the early and intermediate time transient period, the well deliverability is changing and the dynamic p_D function should be used for predicting well rates as discussed in the companion volume, *Well Test Design and Analysis*.

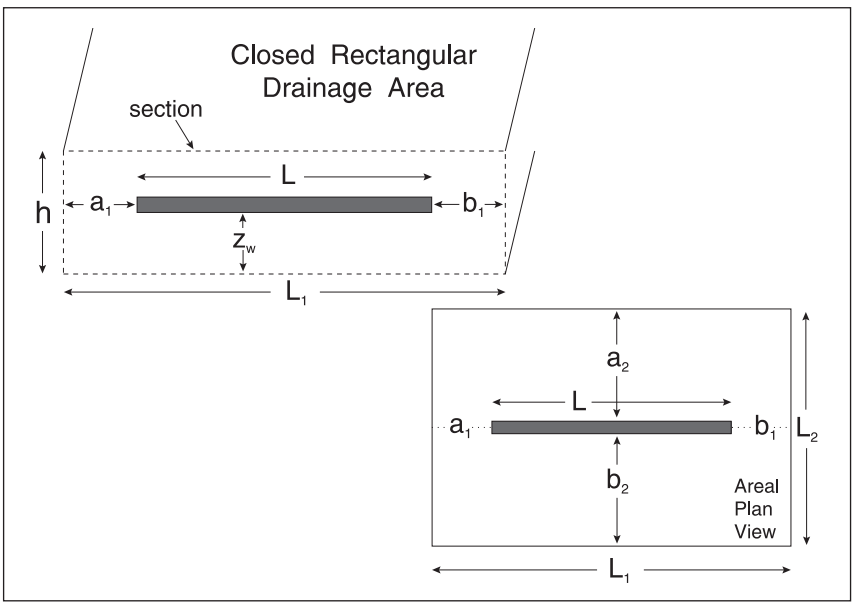

Fig. 1–67. Horizontal well in a closed rectangular drainage area

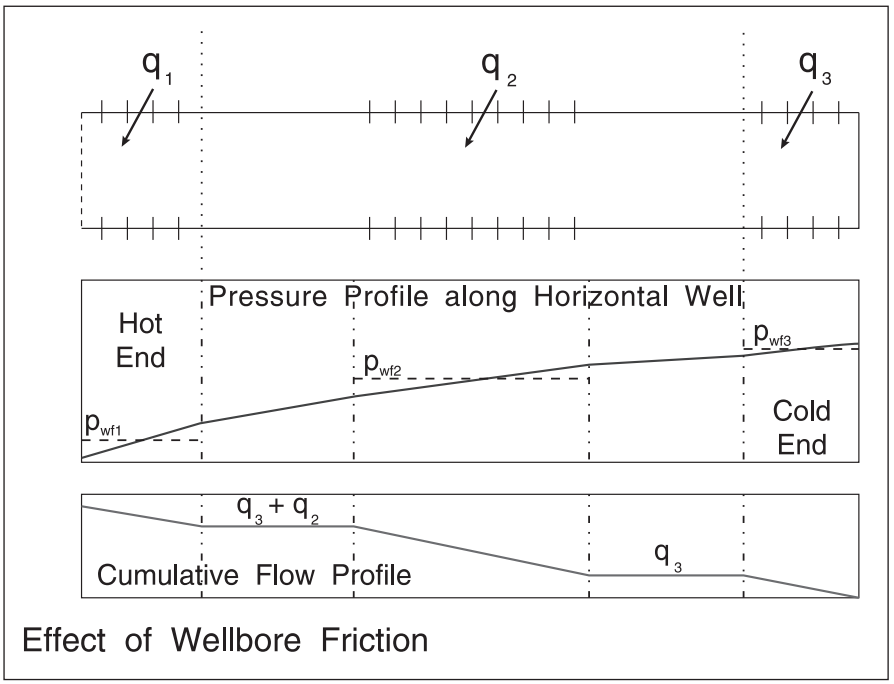

Fig. 1–82. Effect of frictional pressure drop on horizontal well performance

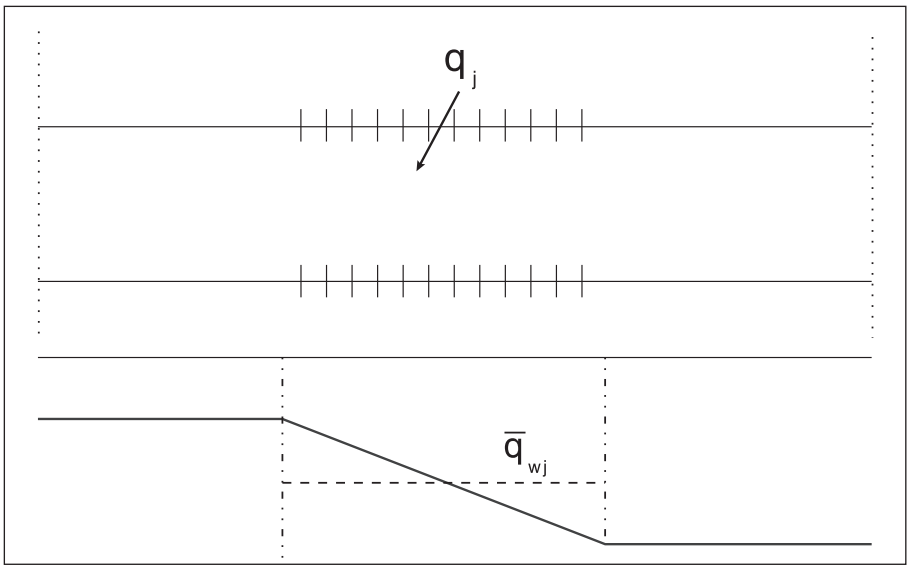

Fig. 1–83. Average wellbore flow-rate over a flowing segment

In the case of single-phase flow, the frictional pressure drop over the flowing length $L_{j,eff}$, is given by the classical formula based on the friction factor f, which is a function of the Reynolds number:

$$\Delta p_{wbf} = \frac{2\rho u^2 f L_{j,eff}}{D} \qquad \textbf{(1–163)}$$

charge is shown in figure 2–1 and the following five main components can be discerned:

- primer
- steel case
- explosive charge
- liner
- cavity

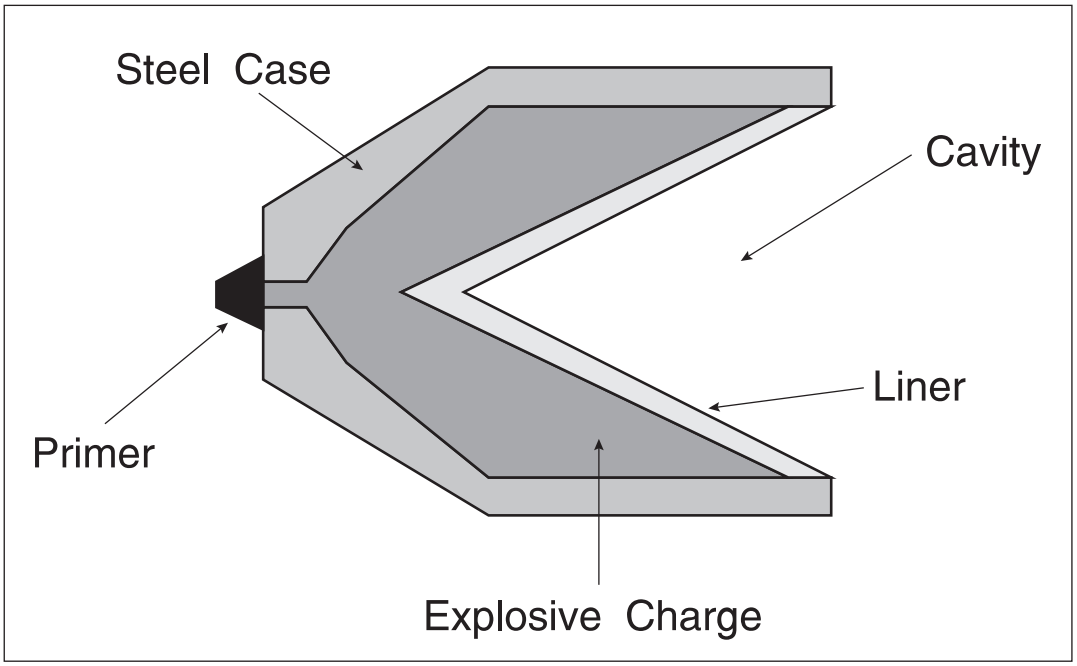

Fig. 2–1. Shaped charge design

Shaped charges come in a wide variety of designs, and the symmetry must be very carefully controlled to ensure the optimal jet effect. Cone axis offset, liner thickness variation, and charge density variation all cause performance deterioration. Quality control during manufacture is therefore crucial to efficient operation. The mechanism of jet perforation is illustrated in figure 2–2, where, after detonation, the liner is now moving towards the target as a liquid jet of approximately 1/16" diameter and a forward velocity of the order of 20,000 ft/s. The pressure exerted on the target is around 5×10^6 psi and a tunnel is driven through casing and cement into the rock by the passage of the slug of liquid like material. The performance of shaped charges is measured in the API—American Petroleum Institute—test denoted RP 43. Here, the charge is fired into a target consisting of a cylinder of Berea sandstone encapsulated by cement in a steel canister as shown in figure 2–3. In order to simulate overbalanced perforation, a 1,500-psi differential towards the target is established, and after perforation a core backpressure of 1,000 psi allows salt water to flow into the system at a pressure differential of 500 psi. The core is then backflushed with kerosene at a differential of 200 psi until stabilization. Since most modern perforation of wells is carried out with underbalance conditions, a reverse flow version of the API test is also carried out; this is illustrated in figure 2–4. In this case, there is a differential of 200 psi towards the “well” side of the target, i.e., the perforation entry face, and after perforation the system is again backflushed with kerosene.